


RESEARCH

Open Access



Comparative assessment of net CO₂ exchange across an urbanization gradient in Korea based on eddy covariance measurements

Je-Woo Hong¹, Jinkyu Hong^{1*} , Junghwa Chun², Yong Hee Lee³, Lim-Seok Chang³, Jae-Bum Lee³, Keewook Yi⁴, Young-San Park⁵, Young-Hwa Byun⁵ and Sangwon Joo⁵

Abstract

Background: It is important to quantify changes in CO₂ sources and sinks with land use and land cover change. In the last several decades, carbon sources and sinks in East Asia have been altered by intensive land cover changes due to rapid economic growth and related urbanization. To understand impact of urbanization on carbon cycle in the monsoon Asia, we analyze net CO₂ exchanges for various land cover types across an urbanization gradient in Korea covering high-rise high-density residential, suburban, cropland, and subtropical forest areas.

Results: Our analysis demonstrates that the urban residential and suburban areas are constant CO₂ sources throughout the year (2.75 and 1.02 kg C m⁻² year⁻¹ at the urban and suburban sites), and the net CO₂ emission indicate impacts of urban vegetation that responds to the seasonal progression of the monsoon. However, the total random uncertainties of measurement are much larger in the urban and suburban areas than at the nonurban sites, which can make it challenging to obtain accurate urban flux measurements. The cropland and forest sites are strong carbon sinks because of a double-cropping system and favorable climate conditions during the study period, respectively (−0.73 and −0.60 kg C m⁻² year⁻¹ at the cropland and forest sites, respectively). The urban area of high population density (15,000 persons km⁻²) shows a relatively weak CO₂ emission rate per capita (0.7 t CO₂ year⁻¹ person⁻¹), especially in winter because of a district heating system and smaller traffic volume. The suburban area shows larger net CO₂ emissions per capita (4.9 t CO₂ year⁻¹ person⁻¹) because of a high traffic volume, despite a smaller building fraction and population density (770 persons km⁻²).

Conclusions: We show that in situ flux observation is challenging because of its larger random uncertainty and this larger uncertainty should be carefully considered in urban studies. Our findings indicate the important role of urban vegetation in the carbon balance and its interaction with the monsoon activity in East Asia. Urban planning in the monsoon Asia must consider interaction on change in the monsoon activity and urban structure and function for sustainable city in a changing climate.

Keywords: Urbanization, Net CO₂ flux, Monsoon, Urban, Suburban, Forest, Cropland, Urban vegetation, East Asia

*Correspondence: jhong@yonsei.ac.kr

¹ Ecosystem-Atmosphere Process Laboratory, Department of Atmospheric Sciences, Yonsei University, Yonsei-ro 50, Seodaemun-gu, Seoul 03722, South Korea

Full list of author information is available at the end of the article



Background

Urbanization and its associated socioeconomic impacts are an essential driver of global climatic and environmental changes. Since the industrial revolution, CO₂ emission by anthropogenic activities (i.e., fossil fuel combustion and land use change) has increased, and the amount of anthropogenic CO₂ emissions has reached 10.7 Gt C year⁻¹ over the last decade [1]. Anthropogenic CO₂ emissions on a continent-to-country spatial scale and annual temporal scale are well known because they correlate with energy consumption data [2], and the magnitude of emissions increases exponentially with the gross domestic product [3, 4]. The ecosystem CO₂ exchanges and surface CO₂ balances on scales with high spatial and temporal resolution, however, involve relatively large uncertainty; thus, they hinder our understanding of the environmental and socioeconomic controlling factors of the spatiotemporal dynamics of the carbon cycle, especially in and around cities. The majority of anthropogenic activity occurs in cities, and cities are where most of the CO₂ emission occurs. Accordingly, we require a better understanding of the carbon sources and sinks in urban areas and their spatiotemporal dynamics for our goal of a sustainable planet.

Human alteration of the Earth's surface, such as urbanization and deforestation for food, fuel, and shelter, overwhelms the magnitude and speed of natural changes and creates an unprecedented impact on land–atmosphere interactions. Land use and cover change (LUCC) is highly involved in urbanization, which is important in local, regional, and global carbon cycles. With rapid urbanization, we are facing extensive LUCC from forest to cropland or city, and it is important that we accurately quantify changes in CO₂ sources and sinks with LUCC in a changing climate. In a natural ecosystem, photosynthesis and respiration are key controlling processes of the carbon and surface energy balances. Vegetative canopy structure (e.g., species, density, ages, and leaf area) and physiological function (e.g., light and water use efficiencies) can explain much of the spatiotemporal variabilities of carbon sources and sinks. However, because of the complexity and heterogeneity of carbon dynamics in the urban canopy, the essential characteristics of land–atmosphere interactions can vary widely across an urbanization gradient, even under the same climatological forcing. Such complexity limits our further assessment of the carbon cycle.

With micrometeorological methods, a number of studies have been monitoring surface CO₂ flux from various land covers over the last three decades, and currently there are more than three hundred monitoring sites across the world. Several limited studies have

been conducted to compare surface CO₂ flux along with urbanization gradient (e.g., [5–8]). Nevertheless, there is a clear gap in the measurements over the urban and suburban areas, croplands, and subtropical forests in the East Asian monsoon region, which prevents us from reducing the uncertainty of surface CO₂ balances in the local, regional, and global carbon cycles. In particular, food and carbon securities are our concern in East Asia because of the rapid urbanization with economic growth, LUCC, and large population density that occur in addition to changes in the monsoon activity and climate. It has been reported that the East Asian monsoon plays a critical role in carbon and energy balances in the terrestrial ecosystem and energy consumption (e.g., [9–11]). Accordingly, our attention should focus on developing efficient policies toward sustainability, considering the substantial alteration of LUCC and monsoon in East Asia. In support of efforts to develop effective carbon adaptation and mitigation policies, this study will provide useful information on changes in the carbon balance in relation to LUCC due to urbanization through a comparative analysis of carbon sources/sinks under monsoon climate conditions.

This study presents eddy covariance measurement data of surface CO₂ fluxes across an urbanization gradient in Korea where the East Asian summer monsoon affects the terrestrial ecosystem and human activity (from urban, suburban, cropland, and subtropical forest sites). In this study, we highlight the change in carbon balance due to a potential change of cropland and forest to an urban area in this critical region.

Methods

Surface CO₂ balance

The surface CO₂ balance over the urban area is given as

$$F_C + dS = C + RE - P \left(\mu\text{mol m}^{-2} \text{s}^{-1} \right) \quad (1)$$

where dS , C , RE , and P are the concentration change of CO₂ in the control volume, CO₂ emission from fossil fuel combustion, respiration by soil, vegetation, and humans, and CO₂ uptake by photosynthesis, respectively. dS can be neglected by the stationary assumption of the eddy covariance method; therefore, the eddy covariance system observes F_C , which is the sum of C , RE , and P in the urban area and corresponds to the net ecosystem exchange of CO₂ (NEE). The impact of C is negligible at stations over natural ecosystems and cropland. The sign convention of micrometeorology is used; therefore, a positive sign indicates net CO₂ flux from the surface to the atmosphere, and a negative sign indicates net CO₂ uptake, presumably via photosynthesis.

Site description

Measurements were taken at four sites in Korea: a high-rise high-density residential area in EunPyeong, Seoul (HU: 37.6350°N, 126.9287°E; Fig. 1a); an open low-rise suburban area in Ochang, Cheongju (SU: 36.7197°N, 127.4344°E; Fig. 1b); a double-cropping rice paddy in Boseong, Jeollanam-do Province (CP: 34.7607°N, 127.2140°E; Fig. 1c); and a subtropical mixed forest on Jeju island (SF: 33.3177°N, 126.5678°E; Fig. 1d) [13]. There is an urban gradient across the sites. Buildings and roads comprised 60% and 36% of land cover at the HU and SU sites, respectively, but were negligible (<1%) at the CP and SF sites. The mean obstacle (i.e., buildings and/or vegetation) height (z_H) is higher at HU (~20 m buildings) and SF (~13.7 m trees) and lower at SU (~4 m buildings) and CP (<1 m of crops) (Table 1). Within a 1 km radius from the SU site, there is a highway and an industrial area that generate CO₂ emissions, which can contribute to the fluxes measured under stable atmospheric conditions. The predominant plant functional types are deciduous broadleaf trees (*Zelkova serrata*, *Cornus officinalis*, etc.) at HU, C3 grasses (*Zoysia japonica*) at SU, C3 crops (*Oryza sativa*: June–November; *Hordeum vulgare*: December–May) at CP, and deciduous broadleaf trees

(*Carpinus tschonoskii*, *Quercus serrata*) at SF. Additional site information has been published previously by Hong and Hong [14] and Hong et al. [15, 16].

The 30-year mean annual precipitation at the five sites is approximately 1240 mm at the SU site, 1450 mm at the HU and CP sites, and 1920 mm at the SF site. The 30-year mean annual air temperature is approximately 12.5 °C at HU and SU, 14 °C at CP, and 17 °C at SF. During the study period, the mean annual precipitation was less than the 30-year average at the HU and SU sites but greater than the 30-year average at the CP and SF sites. More than one-half of the annual precipitation occurred during the summer (June–August) at all sites because of the summer monsoon.

Instrumentation and data analysis

Measurement and data processing

The eddy covariance method was applied to monitor F_C at each site for 1 year from March 2015 to February 2016 (366 days) (Table 1). A 3D sonic anemometer (CSAT-3, Campbell Sci., Logan, UT) and an infrared gas analyzer (IRGA) were installed to measure the wind velocity components, sonic temperature, humidity, and CO₂ concentration. The 10 Hz sampled data were recorded by a data

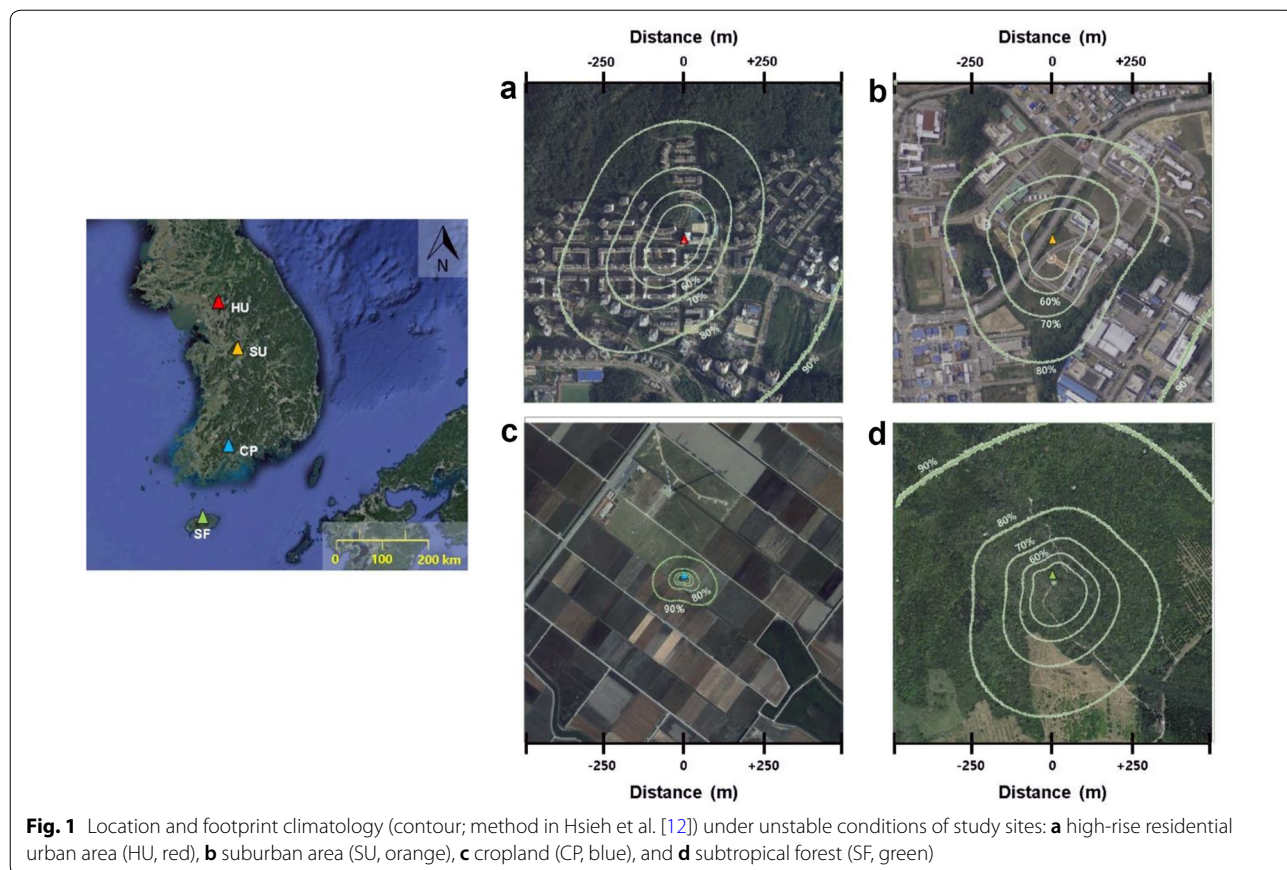


Table 1 Site characteristics and instrumentation details for the study sites

	EunPyeong (HU)	Ochang (SU)	Boseong (CP)	Jeju (SF)
Location				
Latitude (°N)	37.6350	36.7197	34.7607	33.3177
Longitude (°E)	126.9287	127.4344	127.2140	126.5678
Classification	Urban	Suburban	Rice-paddy	Mixed forest
Description	High-density high-rise residential area	Open low-rise research park	Double cropping Dec–May: <i>Hordeum vulgare</i> Jun–Nov: <i>Oryza sativa</i>	Deciduous (82%) <i>Carpinus tschonoskii</i> , <i>Quercus serrata</i>
Population density (km ⁻²)	~15,000	770	<50	~0
Building and road fraction (%)	~60	36	<1	<1
Vegetation fraction (%)	~40	64	~100	~100
Traffic volume (PCU day ⁻¹)	11,549	13,842	–	–
Measurement height (m)	30	19	2.5	27
Obstacle height (m)	~20	~4	<1	~13.7
Altitude (m)	60	60	2	635
Sonic anemometer	CSAT3, Campbell Sci.	CSAT3, Campbell Sci.	CSAT3, Campbell Sci.	CSAT3, Campbell Sci.
Infrared gas analyzer	Li-7200RS, Li-COR	EC-150, Campbell Sci.	EC-150, Campbell Sci.	EC-155, Campbell Sci.
Radiometer	CNR-4, Kipp&Zonen	CNR-4, Kipp&Zonen	CNR-4, Kipp&Zonen	CNR-4, Kipp&Zonen
Data logger	CR-3000, Campbell Sci.	CR-3000, Campbell Sci.	CR-3000, Campbell Sci.	CR-3000, Campbell Sci.
Establishment	May 2013	July 2014	September 2014	May 2014
Analysis period in this study	March 2015–February 2016 (1-year)			

logger (CR-3000, Campbell Sci., Logan, Utah.). A closed-path IRGA was used at HU (Li-7200, Li-COR, Lincoln, NE) and SF (EC-155, Campbell Sci., Logan, UT.), and an open-path IRGA (EC-150, Campbell Sci., Logan, UT.) was used at SU and CP. The 30-min averaged downward/upward short/long-wave radiation was measured by a net radiometer (CNR4, Kipp&Zonen, Netherlands).

Turbulent fluxes were computed using EddyPro software (version 6.2.0, Li-COR, Lincoln, NE) with a 30-min averaging period. Double rotation, spike removal, and spectral correction were applied with a 30-min averaging period. During the postprocessing, outliers in the 30-min CO₂ fluxes were excluded from the data analysis based on median statistics and negative (absorption) CO₂ fluxes during nighttime and nighttime correction is not applied [14, 17].

After quality control, the data availability was approximately 97% for HU, 52% for SU, 63% for CP, and 69% for SF. This study uses Local Standard Time (LST), which is 9 h ahead of Universal Time Coordinated (UTC).

Flux gaps were filled with an artificial neural network (ANN) using MATLAB software. For the ANN, one hidden layer with nine neurons was used with a backpropagation algorithm. The fractions of training data and independent test-set data were 80% and 20%, respectively. The variables used in the gap filling procedure were (1) hour and (2) season (fuzzy system using cosine-transformed time-of-day and day-of-year), (3) 1.5 m

air temperature (T_{air}), (4) 1.5 m relative humidity (RH), (5) 10 m wind speed and (6) direction, (7) downward shortwave radiation, and (8) precipitation. The meteorological variables were obtained from nearby weather observatories for each flux site: Seoul station (37.5714°N, 126.9658°E) for HU, Cheongju station (36.6392°N, 127.4407°E) for SU, Boseong-gun station (34.7633°N, 127.2123°E) for CP, and Seogwipo station (33.2461°N, 126.5653°E) for SF. All meteorological data were processed for quality control in the National Climate Data Portal (<http://data.kma.go.kr/>).

Random flux error estimation

This study evaluates the total random error (ϵ) by applying the 24-h differencing approach [18]. The 24-h differencing approach is a practical method to quantify random flux measurement error if most of the flux towers do not have two towers measuring fluxes over similar vegetation. The 24-h differencing approach calculates the random flux measurement error from measurement pairs on two successive days under the same meteorological conditions [18]. This method has been applied in various ecosystems to estimate the random error of the observed surface fluxes and has provided practical estimates of uncertainty in surface fluxes comparable to those of the sampling error model of Mann and Lenschow [19] and the two-tower approach [18, 20]. Here we will provide a brief introduction to the 24-h differencing

approach; greater detail has been provided by Hollinger and Richardson [18].

If a measurement flux (x) pair of two successive days ($x_1 = F + \varepsilon_1$, $x_2 = F + \varepsilon_2$, where F and ε are the true flux and random error, respectively) is under equivalent meteorological conditions such as radiative flux, air temperature, humidity, and wind speed, the standard deviation of random error ($\sigma(\varepsilon)$) can be written as

$$\sigma(\varepsilon) = \sigma(x_1 - x_2) / \sqrt{2}. \quad (2)$$

For this 24-h differencing method, the similarity of meteorological conditions is defined for 24-h differences in photosynthetically active radiation (PAR) within $75 \mu\text{mol m}^{-2} \text{s}^{-1}$, T_{air} within 3°C , and wind speed within 1 m s^{-1} under no-rainy condition. In addition to these filtering conditions by Richardson et al. [21], the condition of wind direction within $\pm 15^\circ$ was added to consider the surface heterogeneity in wind direction at the sites.

Results and discussion

Climate conditions

The seasonal pattern of climate conditions is similar across the four sites with a seasonal progression of the East Asian summer monsoon (Fig. 2). The annual (March 2015–February 2016) mean T_{air} values are approximately 13.3, 13.8, 14.5, and 16.5°C at HU, SU, CP, and SF, which differ by $+0.8$, $+1.3$, $+0.5$, and -0.5°C from the 30-year average of 1981–2010, respectively. From late June to late July, Korea has “Changma,” the intense heavy rainfall period in summer, and the downward shortwave radiation decreases substantially in this period. It has been reported that this heavy rainfall period imparts a seasonal influence on the carbon and water exchanges of vegetated surfaces in East Asia (e.g., [22, 23]). With this summer monsoon influence, the summertime air temperature is similar across the sites because the same air mass affects the entire Korean Peninsula. In winter, with the retreat of the winter monsoon, there is a temperature difference between the northern sites (HU and SU) and the southern sites (CP and SF) during the study period (Fig. 2a). The annual precipitation is 807, 766, 1281, and $2575 \text{ mm year}^{-1}$ (56%, 62%, 88%, and 134% of the 30-year average) for HU, SU, CP, and SF, respectively, but the timing of rainfall events is similar across the sites. The precipitation differences among the sites are related to the amount of rainfall in the same summer rain events rather than the timing of the rainfall events.

Flux measurement uncertainty

Micrometeorological measurements have several sources of error, including both random and systematic errors that can lead to flux uncertainties. Systematic errors can often be quantified and corrected by regular sensor

calibration. Random errors, however, can grow larger through error propagation and must be quantified in order to conduct a proper data interpretation and model evaluation. We assess the systematic uncertainties in CO_2 fluxes calculated by the different data processing methods. Individual data processing procedures produce nonnegligible uncertainties of approximately 5% of CO_2 fluxes (Table 2). CO_2 fluxes have relatively high sensitivity to detrending methods such as planar fit rotation, outlier removal, and a high-pass filter.

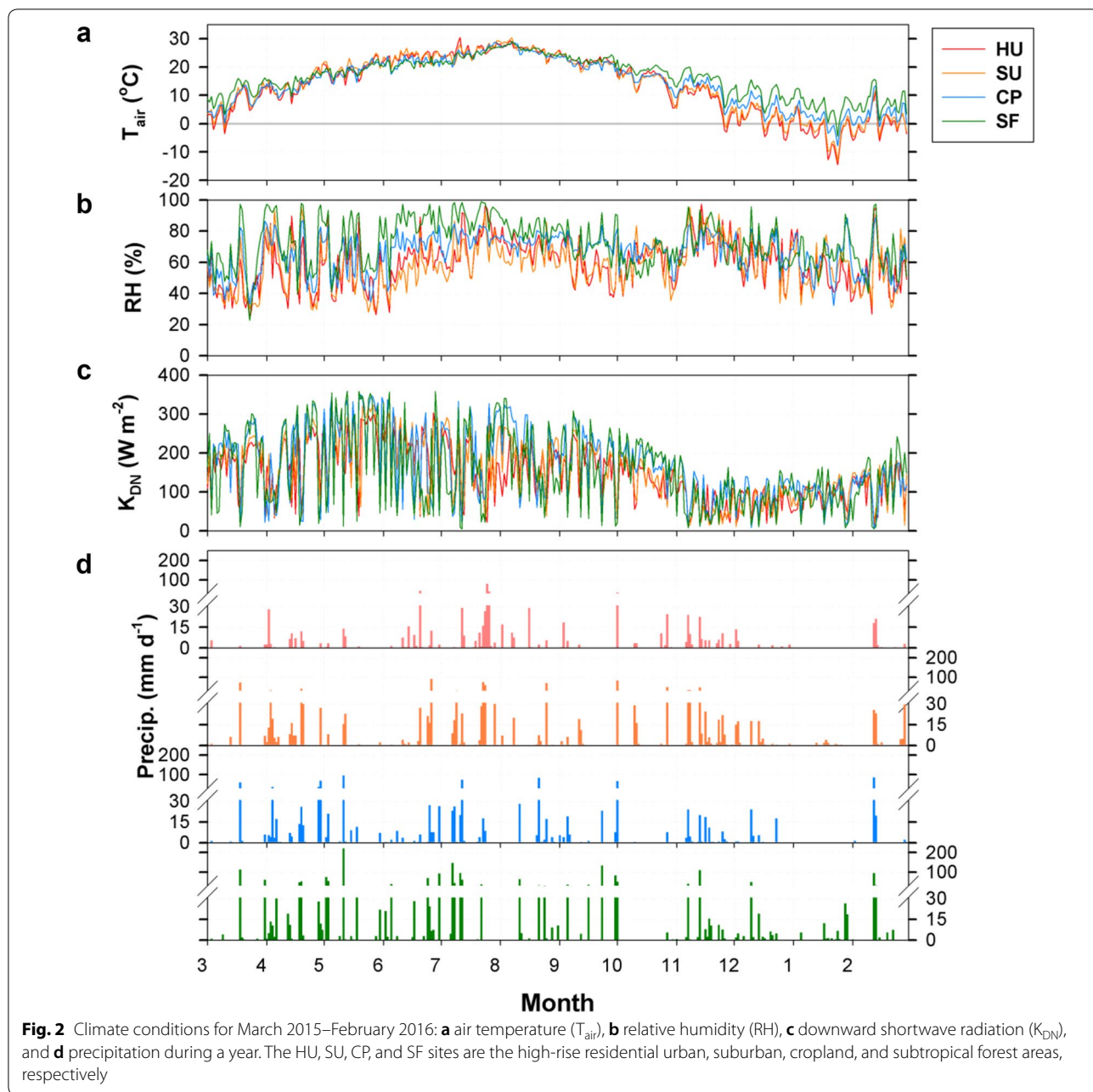
Several general statistical characteristics are robust in the probability density function (PDF) of the random error (ε) of CO_2 flux across the gradient of urbanization and ecosystem types (Fig. 3). First, the probability distribution is symmetrical around the average value with peaky maximum and heavy tails. The Kolmogorov–Smirnov test rejects the hypothesis that the PDF has a Gaussian distribution ($p < 0.01$) and the Laplace (double exponential) distribution is a better approximation than the Gaussian distribution. Indeed, the skewness and kurtosis are large and positive for all sites, such that the PDF deviates significantly from the Gaussian distribution, and they have particularly large values during the nighttime. Our findings are similar to those of previous studies of forest and grass canopies (e.g., [18, 21]).

Second, random flux uncertainty has different variability with turbulent fluxes (i.e., heteroscedasticity) (Fig. 4). The standard deviation of the random error is proportional to the magnitude of the CO_2 flux ($|F_C|$) in all the sites, as calculated via Eq. (3):

$$\sigma(\varepsilon) = a + b|F_C|. \quad (3)$$

The intercept, a , ranges from $-0.02 \mu\text{mol m}^{-2} \text{s}^{-1}$ for the CP site to $1.83 \mu\text{mol m}^{-2} \text{s}^{-1}$ for the HU site. The slope, b , varies between 0.34 and 0.55 across the sites (Table 3). The slope is larger in positive (nighttime) than negative (daytime) CO_2 fluxes in forest and cropland. In contrast, the opposite is true for the urban and suburban sites (i.e., HU and SU). Richardson et al. [20] attributed a larger slope in the daytime compared with nighttime to either data editing or different turbulent transport statistics during the day and night. Positive CO_2 fluxes are, however, possible in the daytime at the HU and SU sites because of the predominance of anthropogenic CO_2 sources. In the case of the HU site, the uncertainty estimation shows similar characteristics even after considering different human activities between weekends and weekdays (not shown here).

In general, our findings are consistent with those of previous studies and indicate that a constant relative error is inappropriate for parameter optimization and data assimilation [21]. The PDFs of random error in the



urban and suburban stations also share similar characteristics with natural vegetation canopies. However, the slope and intercept are larger for the urban-influenced stations (i.e., HU and SU) than for cropland and forest (i.e., CP and SF), indicating that random flux uncertainties are much larger in an urban area than in natural forest or cropland. Although our estimation was generated by dividing wind direction into narrow ranges, the surface heterogeneity of urban structure and function and the larger relative error will have potential impacts on

random error variability. Another plausible explanation for this larger relative random error is that anthropogenic activity is not mainly controlled by meteorological conditions, thus invalidating the 24-h differencing approach in the HU site.

Temporal dynamics of CO₂ flux along the urbanization gradient

There are distinct differences in net CO₂ fluxes among the sites across the gradient of urbanization from the

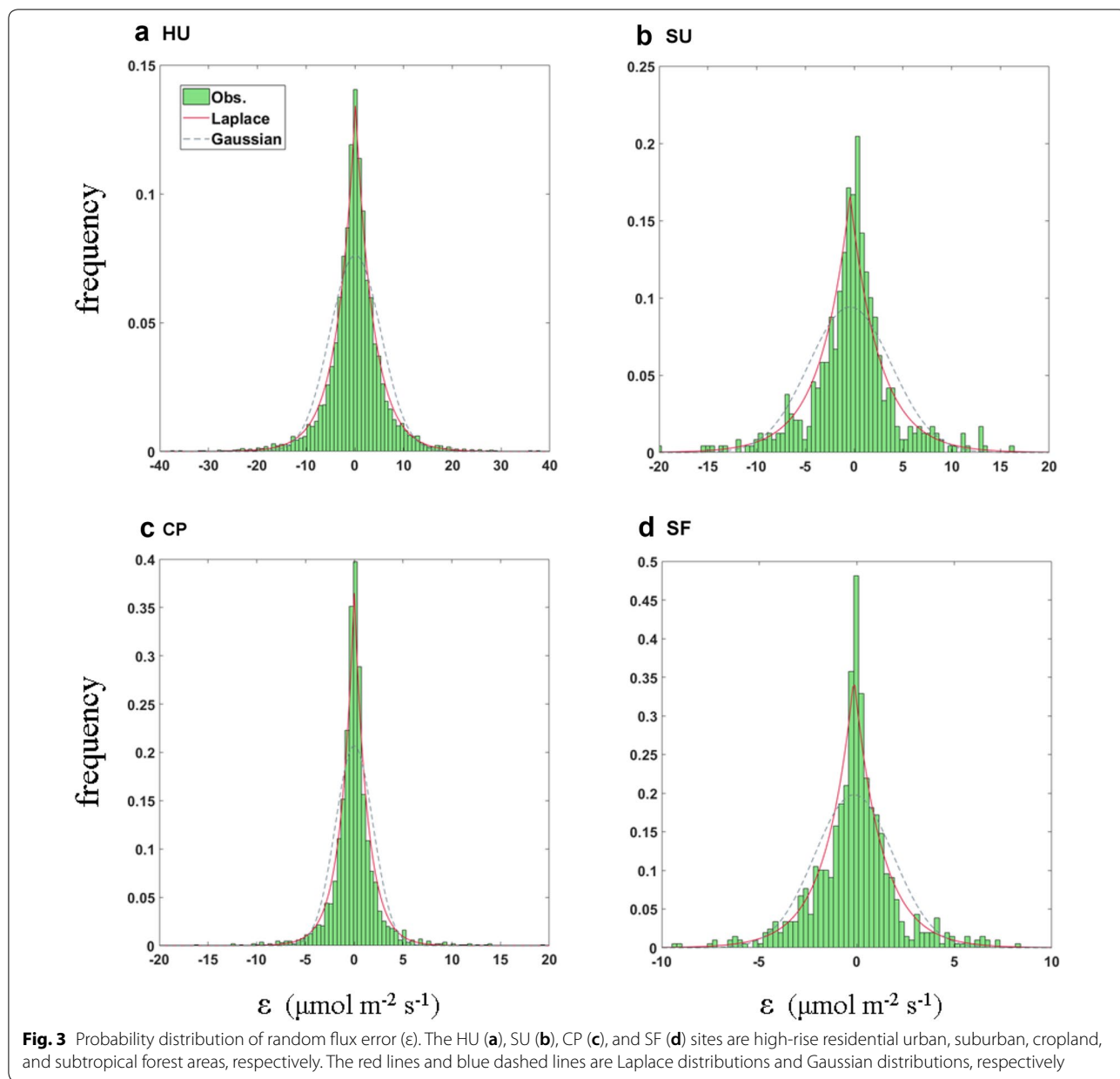
Table 2 CO₂ fluxes and their uncertainties with different processing procedures

F_C (unit: $\mu\text{mol m}^{-2} \text{s}^{-1}$)	Mean	Std.	25%	50%	75%
Default (<i>double rotation & block averaging only</i>)	8.8	7.3	2.3	7.8	14.4
Difference with default (EXP-default; unit: $\mu\text{mol m}^{-2} \text{s}^{-1}$)					
Coordinate rotation					
Triple rotation	-0.1	1.5	0.0	0.0	0.1
Planar fit [24]	-0.8	3.8	-1.7	-0.5	0.3
Planar fit [25]	-1.0	3.9	-1.9	-0.6	0.3
Detrending					
Linear detrending	-0.4	3.9	-1.3	-0.1	0.4
Running mean 250 s	-0.7	4.3	-2.0	-0.5	0.8
Exponential running mean 250 s	-0.9	3.8	-2.0	-0.6	0.2
Time Lags Compensation					
Covariance maximization	0.0	0.1	0.0	0.0	0.1
<i>Covariance maximization with default</i>	0.1	0.1	0.0	0.0	0.1
Automatic time lag Optimization	0.0	0.1	0.0	0.0	0.1
Spike count/removal					
Mauder et al. [26], accepted spikes 1–30%	-0.5	1.4	-0.3	0.0	0.0
<i>Vickers and Mahrt [27] (VM97), Max consecutive outliers (MCO) 3</i>	-0.1	0.2	-0.1	0.0	0.0
VM97, MCO 10	-0.2	0.4	-0.2	0.0	0.0
VM97, MCO 30	-0.3	0.7	-0.4	-0.1	0.0
VM97, MCO 50	-0.4	0.8	-0.4	-0.1	0.0
VM97, MCO 70	-0.4	0.8	-0.5	-0.1	0.0
Amplitude resolution					
4–7 sigma, number of bins 50–150	0.0	0.1	0.0	0.0	0.1
Dropouts					
Accepted central dropouts 5–20%	0.0	0.1	0.0	0.0	0.1
Absolute limits	0.0	0.1	0.0	0.0	0.1
Skewness & Kurtosis	0.0	0.1	0.0	0.0	0.1
Discontinuities	0.0	0.1	0.0	0.0	0.1
Spectral correction					
<i>Low-frequency range [28]</i>	0.3	0.4	0.1	0.2	0.4
High-frequency range (HFR) [29]	0.1	0.2	0.0	0.1	0.2
HFR [30, 31]	0.7	1.0	0.2	0.4	0.8
HFR [32]	0.2	0.3	0.0	0.1	0.4
HFR [33] with Horst and Lenschow [34] (HL09): along-wind, cross, and vertical winds	0.1	0.2	0.0	0.1	0.2
HFR [33] with HL09: only cross and vertical winds	0.1	0.1	0.0	0.1	0.2
HFR [35] with HL09: along-wind, cross, and vertical winds	0.2	0.2	0.0	0.1	0.3
<i>HFR [35] with HL09: only cross and vertical winds</i>	0.2	0.2	0.0	0.1	0.3

Data period is 1-month (March 2015) from HU site. *Italic* indicates the methods applied in this study

perspectives of diurnal and seasonal variations of net CO₂ exchange (Figs. 5 and 6). The SF site is a strong CO₂ sink from the end of April through October, and the maximum CO₂ absorption rate is $-25 \mu\text{mol m}^{-2} \text{s}^{-1}$ during this period (Figs. 5d and 6d). Importantly, during the summer growing season, the SF site shows an obvious mid-season decline of carbon uptake with a substantial reduction in the solar radiation. In other words, the

forest site exhibits strong carbon uptake after the leaf-out in early May, which significantly decreases with the onset of the summer monsoon and regains its strong carbon uptake on non-rainy summer days. The carbon uptake in the forest canopy continues until defoliation in late October. Such a bimodal peak of NEE is a typical seasonal variation in forest canopies that is influenced by the Asian summer monsoon (Figs. 5d and 6d) (e.g., [9, 22]).



The cropland also shows a bimodal peak of carbon uptake but in a different period from the forest (from April to August) because of a double-cropping farming system (planting and subsequent harvest of barley and rice). NEE shows rapid changes in sign during the harvest of crops in June (barley) and November (rice) at the CP site. The maximum CO_2 absorption rate is approximately $-40 \mu\text{mol m}^{-2} \text{s}^{-1}$ for rice in July–August, which is comparable to previous results from rice paddies in East Asian countries (e.g., [36–40]). The maximum CO_2 absorption rate of barley is smaller (approximately

$-20 \mu\text{mol m}^{-2} \text{s}^{-1}$) during the mid-growing period of barley (from April to May).

Unlike the forest and cropland, the HU and suburban (SU) areas are sources of CO_2 to the atmosphere throughout the year, and the seasonal variability of CO_2 flux is relatively small compared with the cropland and forest. Nonetheless, we can see the influence of the heavy rain period in summer, possibly because of urban vegetated surfaces at both the urban-influenced sites (Fig. 5). Indeed, the suburban area exhibits daytime carbon uptake (i.e., negative CO_2 flux) in the summer growing season (from March to October). The urban site does not

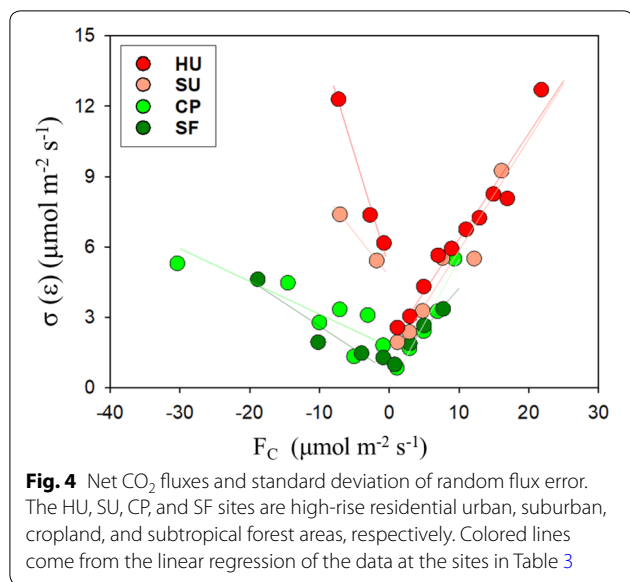


Table 3 The linear relationship between random flux error and the corresponding flux magnitude

Site	$F_c \leq 0$	$F_c \geq 0$
HU	$-0.97 \times F_c + 5.11$ (0.99)	$0.45 \times F_c + 1.83$ (0.95)
SU	$-0.37 \times F_c + 4.75$ (1.00)	$0.48 \times F_c + 1.11$ (0.92)
CP	$-0.14 \times F_c + 1.74$ (0.69)	$0.55 \times F_c - 0.02$ (0.95)
SF	$-0.20 \times F_c + 0.67$ (0.89)	$0.34 \times F_c + 0.82$ (0.99)

The number in the parentheses indicates the correlation coefficient

show negative fluxes even in the summer, but the positive CO₂ fluxes do decrease in a similar manner as at the suburban site in the summer.

Figure 6 shows the diurnal variation of CO₂ flux. Two peaks of CO₂ flux are evident, during the morning and evening rush hours at HU. However, in the suburban area, vegetated surfaces in the flux footprint offset the afternoon rush hour effect, and the maximum carbon uptake occurs around noon when the solar radiation is at its maximum. Traffic volumes at HU and SU show the similar diurnal pattern with rush hour peaks and SU has larger traffic volume than HU (Table 1). Consequently, the maximum CO₂ emission rate of the SU site is half that at the HU site (approximately 10 μmol m⁻² s⁻¹), and its timing is delayed to the late evening despite the larger traffic volume at SU. It is also notable that these two peaks in the rush hours become smaller during the summer season, indicating that vegetated surfaces mitigate anthropogenic CO₂ emissions in the summer growing season. The seasonal variation of anthropogenic CO₂ emission at the HU and SU sites are relatively small possibly because of the district (HU site) and electricity (SU site) heating

system not to make anthropogenic CO₂ emission. In this respect, the seasonal course of CO₂ flux shows a mid-season depression of CO₂ absorption, with two minima around May and September in the urban and suburban areas, with the combination of vegetative uptake and the lengthy summer monsoon period as the vegetative carbon uptake decreases in July during heavy summer rain spells. Previous studies reported that such a mid-season depression is related to the effect of heavy rain spells on ecosystem function in the Asian summer monsoon season (e.g., [9, 23]). Our result suggests that the interplay of urban vegetation and summer monsoon activity and CO₂ flux in cities in the East Asian monsoon region should also be interpreted with the seasonal progression of the East Asian monsoon similarly to natural vegetation in this region.

Light use efficiency of CO₂ fluxes

Figure 7 shows the light-response curve during the growing season: May–September for urban, suburban, and forest sites; and April–May for barley and July–September for rice at the cropland site. All the sites except for HU tend to increase CO₂ uptake from the atmosphere (i.e., negative F_c) as PAR increases. The cropland and forest sites show increases in carbon uptake with increasing PAR that are similar to previous reports for various vegetative canopies (e.g., [41, 42]). In the rice paddy, the photosynthesis rate continues to increase as PAR intensifies without the light saturation, thus leading to larger light use efficiency (LUE) compared with the forest. We speculate that this large LUE is related to the ample nutrients and water supplied to the rice paddy by fertilization and irrigation.

The suburban site shows the typical pattern of vegetative canopies as LUE increases. However, in the SU site, a positive F_c is maintained up to a relatively large PAR of approximately 500 μmol m⁻² s⁻¹, as compared with other natural canopies. This suggests that the sign change of F_c from positive to negative with higher PAR is related to the compensation of CO₂ emission by vegetation around the tower. The net CO₂ emission rate at the high-rise residential site does not change significantly regardless of PAR variation and shows two peaks during the rush hours corresponding to approximately 600 and 1300 μmol m⁻² s⁻¹ in PAR. These results indicate the predominance of carbon emission from cars, which does not depend on temperature. It is also noticeable that CO₂ fluxes with small PAR are larger at the urban-influenced sites (HU and SU) than at those with vegetative canopies (CP and SF), but they are much smaller than in other cities reported by Ward et al. [7].

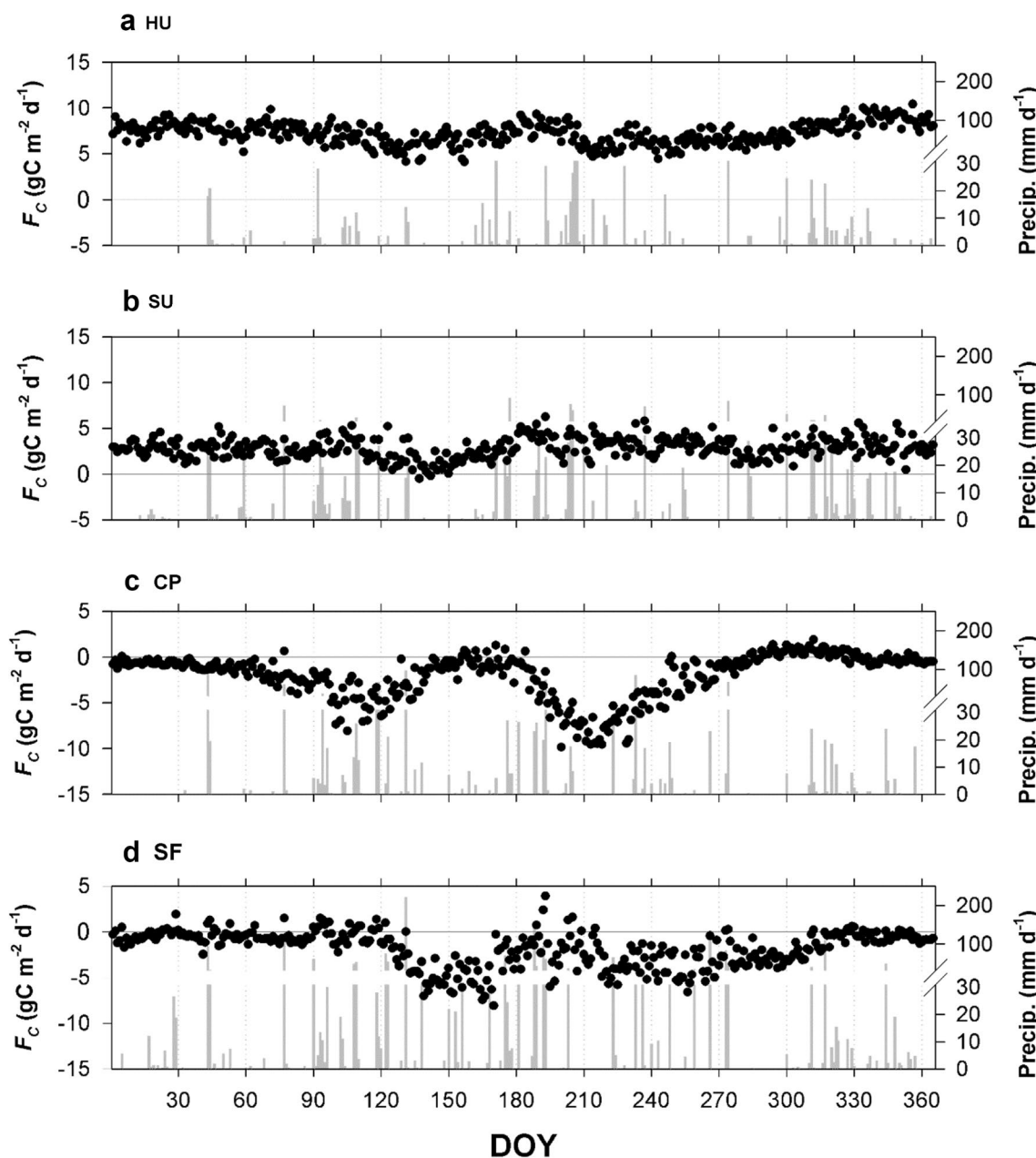


Fig. 5 Daily CO₂ fluxes and precipitation at **a** high-rise residential urban (HU), **b** suburban (SU), **c** cropland (CP), and **d** subtropical forest (SF) sites from March 2015 to February 2016

Temperature responses of CO₂ flux

Figure 8 is a nighttime temperature-response curve of CO₂ flux. It has been reported that in natural ecosystems, nighttime CO₂ flux is an exponential function of T_{air} because warmer temperature creates favorable conditions for ecosystem respiration [43, 44]. Our results also show this typical dependency of nocturnal F_c on T_{air} except for the HU area. The HU area exhibits the typical

temperature dependence only in the summer season (> 20 °C range) and shows nearly constant CO₂ flux with changes in T_{air} indicating possible contribution of ecosystem respiration in summer at the urban residential area.

Net carbon emission is nearly constant throughout the year at the HU and SU sites, and CO₂ emissions do not show significant variations with changes in T_{air} (Fig. 9). It is mainly because of (1) the power plant is located out of

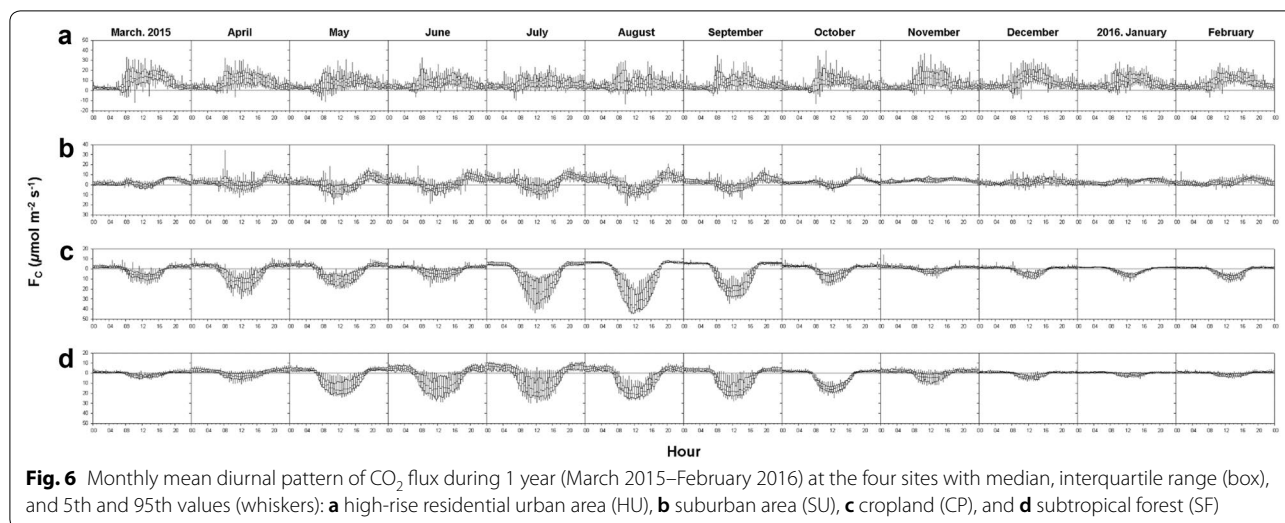


Fig. 6 Monthly mean diurnal pattern of CO₂ flux during 1 year (March 2015–February 2016) at the four sites with median, interquartile range (box), and 5th and 95th values (whiskers): **a** high-rise residential urban area (HU), **b** suburban area (SU), **c** cropland (CP), and **d** subtropical forest (SF)

the source area and (2) both sites are using the heating system without CO₂ emissions, leading to nearly constant anthropogenic activities. Compared with the crop and forest canopies, the temperature-response curve for nocturnal CO₂ flux has a relatively wider range at the urban and suburban sites, and the mean values are larger than the medians with increases in urbanization (i.e., positive skewness) (Fig. 8). Anthropogenic emissions exhibit more asymmetry in their diurnal trends than emissions from plants and soils because anthropogenic activities such as heating and transportation tend to be higher in the afternoon than in the morning, given the air temperature at the HU and SU sites (Fig. 6), suggesting that the observed CO₂ fluxes at the HU and SU sites reflect strong anthropogenic CO₂. The baseline of the $F_c - T_{air}$ relationship at the HU site is larger than at the other three sites (approximately 5 $\mu\text{mol m}^{-2} \text{s}^{-1}$) but smaller than in other cities (about 50 $\mu\text{mol m}^{-2} \text{s}^{-1}$ in city center of London,

about 10 $\mu\text{mol m}^{-2} \text{s}^{-1}$ in the Swindon suburban site [7]; and about 20 $\mu\text{mol m}^{-2} \text{s}^{-1}$ in Beijing, China [45]).

CP and SF sites show a larger spread of the distribution of CO₂ flux with warm air temperatures (15–20 °C for CP and above 20 °C for SF). For the forest canopy (SF), warm climate conditions of > 20 °C correspond to the summer growing season (May–October) and include the heavy rain spell, Changma (late June–late July). This result shows that ecosystem respiration in summer is sensitive to the timing and duration of rainfall events during the Changma, creating larger variability through substantial variations of the downward shortwave radiation and surface moisture in this region [22, 23]. On the contrary, it is not obvious that the seasonal progression of the monsoon makes such an impact on the crops, probably because of the human management of the rice paddy. Instead, it is observed that abrupt changes in vegetative surfaces occur during the harvest of barley and during the planting (May) and harvest (October) of rice, and such periods match up with large uncertainties in ecosystem respiration in the range of 15–20 °C (Fig. 8c).

Monthly average CO₂ fluxes produce negative relationships because of the carbon uptake in summer (Fig. 9). It is notable that the HU (−0.05 $\mu\text{mol m}^{-2} \text{s}^{-1} \text{ } ^\circ\text{C}^{-1}$) and SU (−0.02 $\mu\text{mol m}^{-2} \text{s}^{-1} \text{ } ^\circ\text{C}^{-1}$) sites produce a less steep negative slope between T_{air} and F_c compared with other cities in previous studies (−0.56 and −1.95 $\mu\text{mol m}^{-2} \text{s}^{-1} \text{ } ^\circ\text{C}^{-1}$ at Swindon and London, UK [7]; −0.34 $\mu\text{mol m}^{-2} \text{s}^{-1} \text{ } ^\circ\text{C}^{-1}$ in Beijing, China [45]; −0.25 $\mu\text{mol m}^{-2} \text{s}^{-1} \text{ } ^\circ\text{C}^{-1}$ in Tokyo, Japan [46], 2004; and −0.2 $\mu\text{mol m}^{-2} \text{s}^{-1} \text{ } ^\circ\text{C}^{-1}$ in Łódź, Poland [47]). Around the HU site, the high-rise residential buildings use a district heating system, which uses hot water coming through pipes from remote power plants. In contrast, the

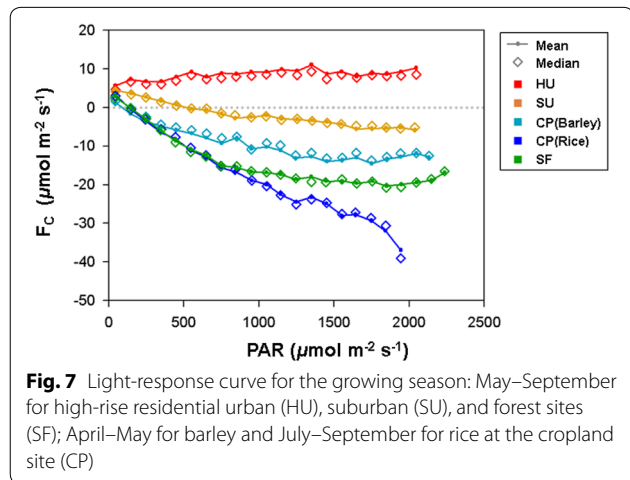
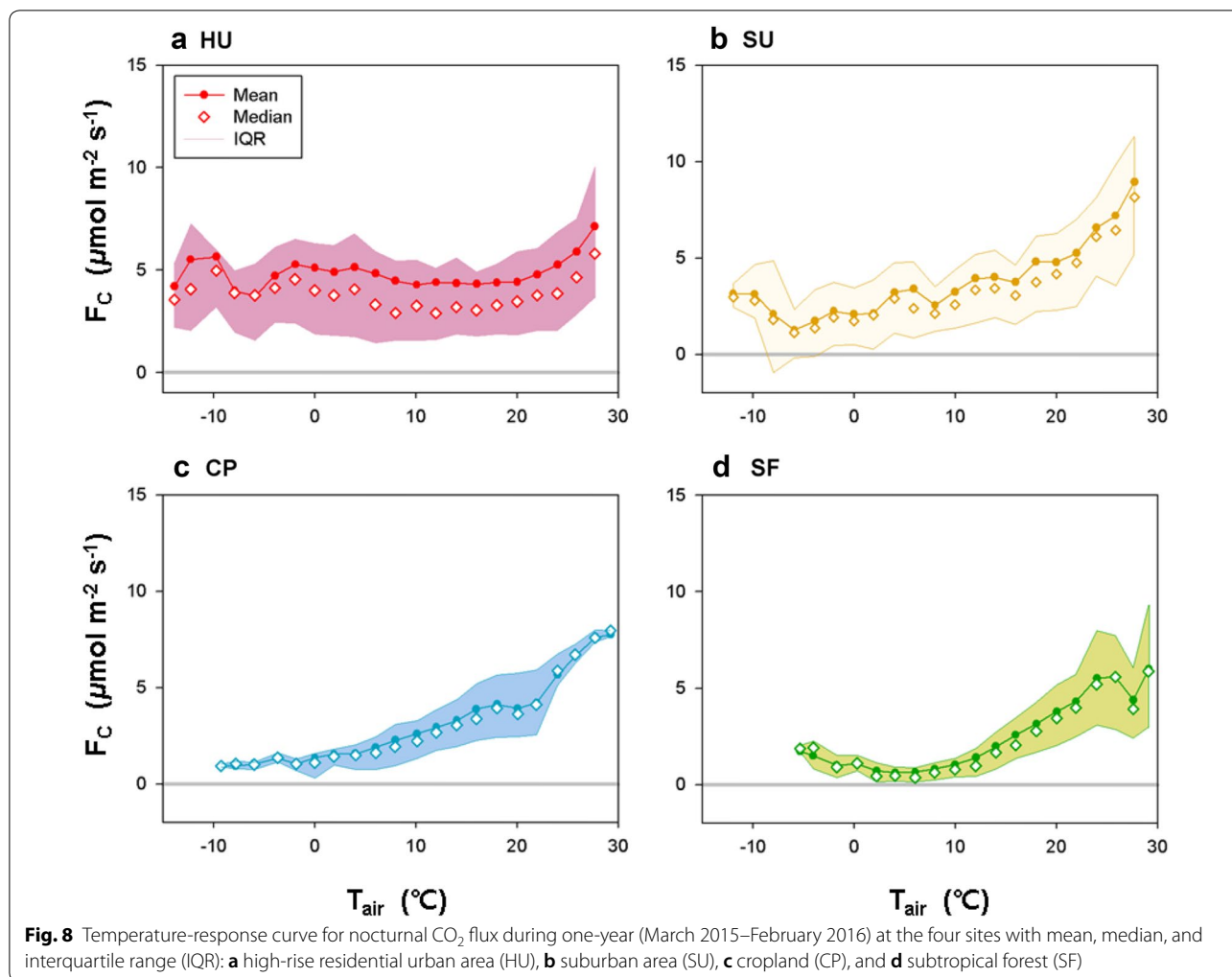


Fig. 7 Light-response curve for the growing season: May–September for high-rise residential urban (HU), suburban (SU), and forest sites (SF); April–May for barley and July–September for rice at the cropland site (CP)



houses and buildings around the SU site usually use electricity for heating. In addition, the resident population is small (<700 people km⁻²), and the vegetated surface mitigates fossil fuel emissions through photosynthesis. Consequently, these societal environments around the HU and SU stations do not contribute to the local CO₂ emissions, thus producing a relatively weak negative correlation compared with the previous studies. In contrast, there is a strong seasonal variation in CO₂ fluxes at the cropland and forest canopy sites, with the seasonality of vegetation shown in the light-response curve (Fig. 7).

Annual net CO₂ fluxes

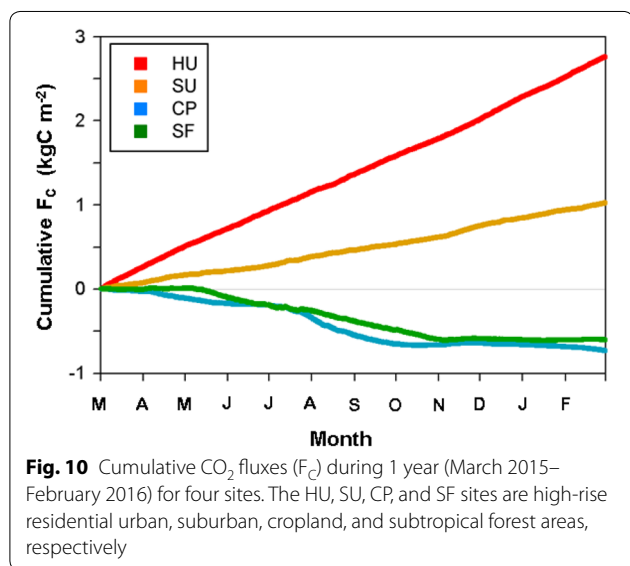
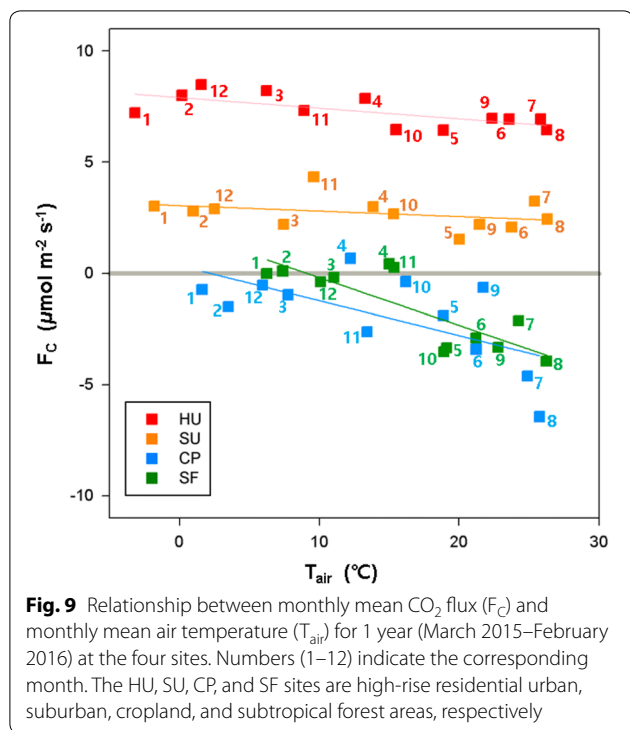
The annual net CO₂ fluxes are 2.75, 1.02, -0.73, and -0.60 kg C m⁻² year⁻¹ for the urban, suburban, cropland, and forest sites, respectively. The urban and suburban sites are carbon sources to the atmosphere throughout the year and show monotonically increasing

cumulative CO₂ fluxes because of the weak seasonality (Fig. 10).

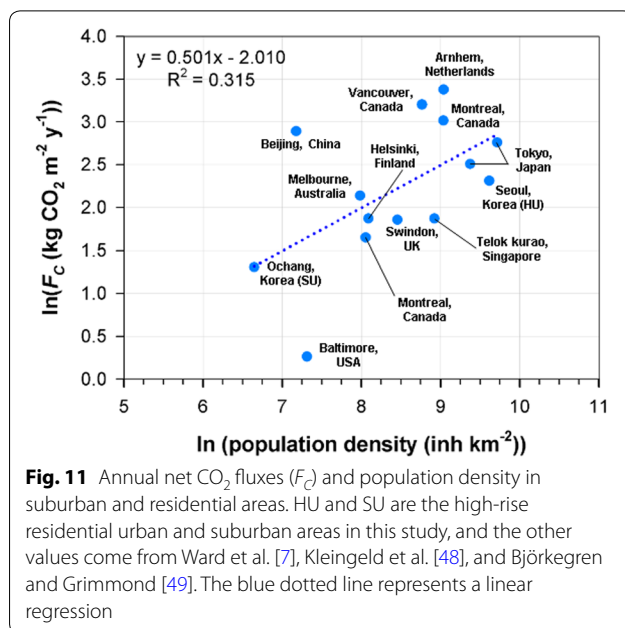
Figure 11 shows CO₂ fluxes in suburban and residential areas vs. population density. In general, net CO₂ flux in a suburban and urban residential area has sublinear scaling with population density (*P*; number of inhabitants per km², inh km⁻²) on a logarithmic scale:

$$F_c = F_{c_0} \cdot P^\alpha \tag{4}$$

where *F_{c0}* is net CO₂ flux at a zero population of 0.13 kg CO₂ m⁻² year⁻¹ and *α* is the scaling exponent of 0.50 from the linear regression with *R*=0.56. In other words, the relationship exhibits sublinear scaling (*α* < 1), and therefore a larger urban population density is more efficient with regard to net CO₂ flux. However, this sub-linear relationship has a smaller correlation coefficient (i.e., a wide spread of CO₂ flux at the given population density) and a less steep slope compared with inventory data analysis. For example, Fragkias et al. [50] reported



a slope of 0.93 with $R=0.99$ in US cities, and the top 500 CO₂-emitting cities reported in Moran et al. [51] had a slope of 0.72 with $R=0.93$ (calculated in this study based on their data). Anthropogenic CO₂ emission around HU and SU are 6.0 and 3.3 kg C m⁻² year⁻¹ from the ODIAC emission dataset [52]. If we consider that our measurement includes both fossil fuel emissions and vegetative carbon uptake, our result suggests that urban vegetation



is important to offset anthropogenic emissions in urban areas; thus, the net CO₂ flux for cities will depend on population density, traffic volume, and vegetation cover fraction.

Indeed, the net CO₂ emissions per capita at the urban (HU) and suburban (SU) sites were 0.7 and 4.9 t CO₂ year⁻¹ person⁻¹, respectively, and they scale with population density similarly to other cities (Fig. 11, Table 4). The HU site shows a smaller CO₂ emission rate than Tokyo, Japan, which has a similar population density and vegetation fraction [46, 55]. It is notable that the vegetation cover can partially explain the outliers from this subsampling (Fig. 12). The smaller CO₂ emission rate at HU can be attributed to the larger vegetation fraction compared with Tokyo, Japan. The higher CO₂ emission rate per capita in Beijing, China also corresponds to a smaller vegetation fraction (<20%). It is noticeable that the large CO₂ emission rates per capita (>0.65 t C year⁻¹ inh⁻¹) in Vancouver and Montreal, Canada [6, 56] and Arnhem, Netherlands [48] are scaled well with changes in vegetation fraction but are much stronger than other cities. We speculate that major CO₂ sources of these sites are from space-heating systems and low vegetation fraction (Fig. 12b).

The CO₂ emission rate in HU site is also smaller than the inventory values (about 12 t CO₂ year⁻¹ inh⁻¹) on the regional scale around the Seoul metropolitan area [51, 57]. It has been reported that typical uncertainties of the inventory-based emission estimates are smaller (<10%) in national to global scales but larger (<30%) in city scale [58–61]. In particular, the anthropogenic emission has

Table 4 Annual net CO₂ fluxes (F_c) from suburban and urban residential areas in the literature

Location	Vegetation fraction, F _v (%)	Population density, P (inh km ⁻²)	F _c (kg CO ₂ m ⁻² year ⁻¹)	F _c /P (t C year ⁻¹ inh ⁻¹)	References
Seoul, Korea	40	15,000	10.1	0.18	This study
Ochang, Korea	64	770	3.7	1.31	This study
Tokyo, Japan	21	11,800	12.3	0.28	[52]
Tokyo, Japan	5.5 ^a	16,600	15.8	0.26	[55]
Beijing, China	15	1309	18.0	3.75	[58]
Singapore	15	7491	6.5	0.24	[53]
Melbourne, Australia	38	2939	8.5	0.79	[5]
Helsinki, Finland	44	3262	6.5	0.54	[54]
Arnhem, Netherlands	12	8425	29.3	0.95	[48]
Swindon, UK	44	4700	6.4	0.37	[7]
Vancouver, Canada	35	6420	24.6	1.05	[56]
Montreal, Canada (URB)	29	8400	20.4	0.66	[6]
Montreal, Canada (SUB)	50	3150	5.2	0.45	
Baltimore, USA	67	1500	1.3	0.24	[61]

^a Vegetation fractions in summer and winter are equally averaged

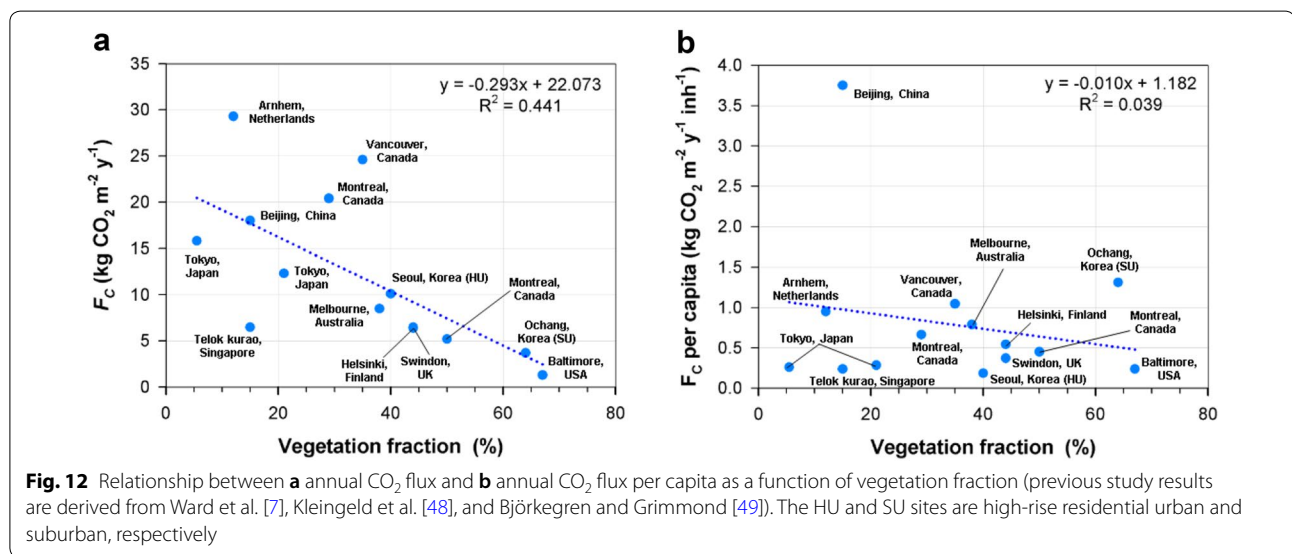


Fig. 12 Relationship between **a** annual CO₂ flux and **b** annual CO₂ flux per capita as a function of vegetation fraction (previous study results are derived from Ward et al. [7], Kleingeld et al. [48], and Björkegren and Grimmond [49]). The HU and SU sites are high-rise residential urban and suburban, respectively

large uncertainties at the outskirts of the city such as the HU and SU sites [60]. The smaller observed CO₂ emission rate is also attributable to the spatio-temporal mismatch of heating system, traffic amount, and vegetation activities between the inventory-based emission estimates and in situ flux measurements. Indeed, the power plant contribution is not in the flux footprint unlikely to the area wide inventory-based emission estimates.

The net CO₂ emission at the SU site obeys the scaling relationship given by Eq. (4) but shows larger CO₂ emission than Baltimore, USA, which has a similar vegetation fraction (>0.5) but a larger population density [62]. In

addition, despite the smaller population density and the larger vegetation fraction around the SU site, the traffic volume around the SU site is larger than around the HU site; therefore, heavy traffic volumes and factories in the suburban area contribute to additional CO₂ emissions into the atmosphere. Because urban CO₂ emissions can be interpreted by a measure of energy consumption and traffic volume, it is likely that the district heating system around the HU site contributes a much smaller net CO₂ emission compared with the SU site. This finding is consistent with the results of Makido et al. [63], who reported less CO₂ emission from the passenger

transportation sector from compact cities compared with more sprawling cities and a less steep slope of F_c to T_{air} in the urban and suburban areas (Fig. 9).

The annual mean CO_2 fluxes of the four sites and the controlling factors are comparable to those of previous studies: e.g., traffic volume and vegetation fraction in urban areas [7, 8, 63] and air temperature and precipitation in crops and natural vegetation canopies in various climate zones [64–68] (Figs. 12 and 13). Our results for the HU and SU sites are also within the range of the relationship between carbon emissions and vegetation fraction reported by Ward et al. [7] and Lietzke et al. [69] (Fig. 12).

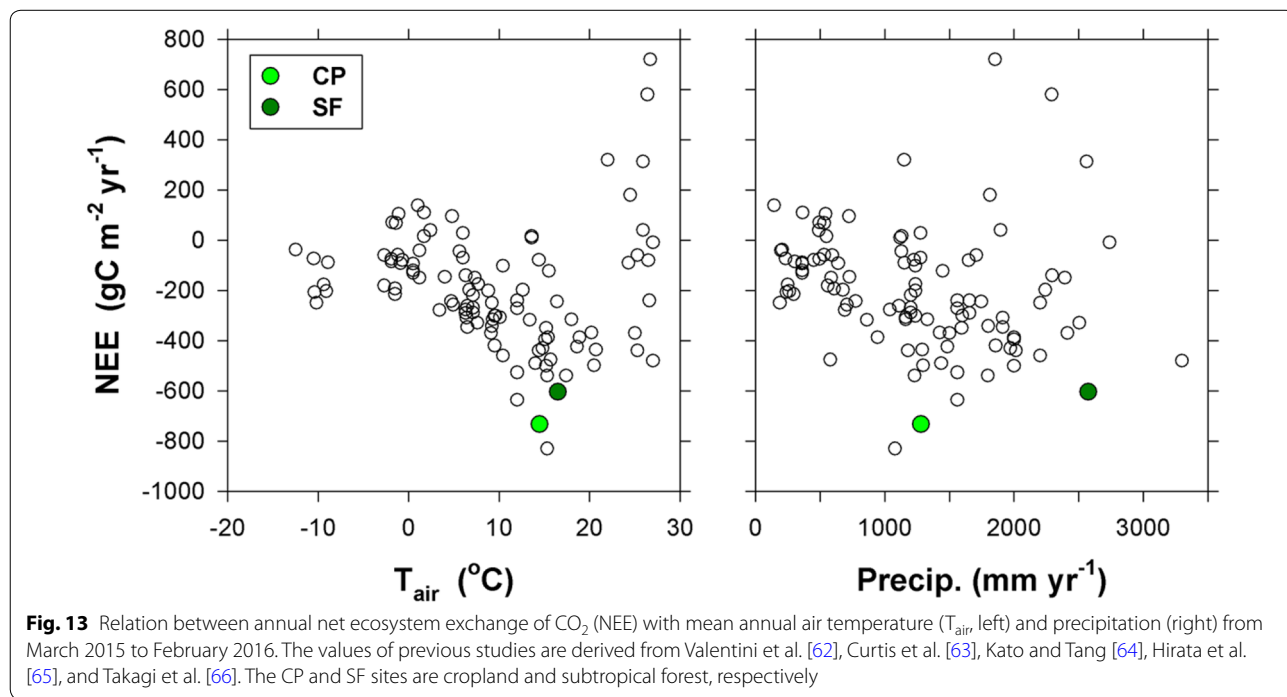
The CP and SF sites are strong carbon sinks compared with other vegetation canopies (Fig. 13). In particular, the CO_2 uptake of the cropland is large because the double-cropping system and human management alleviate the effects of the heavy rain spells in summer, thus producing larger carbon uptakes in spring and summer with $T_{air} > 10\text{ }^\circ C$. The slopes of carbon uptake accumulation corroborate this, indicating the effect of human intervention in the cropland (Fig. 9). Some possible causes of such a relatively large amount of net carbon uptake in SF are (1) young forest ages (31–50 years), (2) abundant water due to precipitation, (3) relatively weaker disturbance of the summer monsoon during the study period, and (4) warm winter conditions leading to additional photosynthesis in the evergreen forest canopy in winter. Only a few sites in Asia have recorded annual NEE

values that are comparable to the cropland and forest sites in this study: (1) $-0.64\text{ kg C m}^{-2}\text{ year}^{-1}$ in a mixed forest in Japan (34.7833°N, 135.8500°E; no climate information) [70], (2) $-0.83\text{ kg C m}^{-2}\text{ year}^{-1}$ in a mixed forest in Japan (34.7333°N, 134.3667°E; annual precipitation 1078 mm year⁻¹, annual mean T_{air} 15.3°C) [71], and (3) $-0.64\text{ kg C m}^{-2}\text{ year}^{-1}$ in a fertilized rangeland in Japan (36.9167°N, 139.9667°E; 1561 mm year⁻¹, 12.0 °C) [72].

Conclusions

This study analyzes eddy covariance measurements of CO_2 fluxes at the land–atmosphere interface across an urbanization gradient in Korea with high-rise high-density urban residential, suburban, double-cropping cropland, and forest canopy areas. Our study shows that the systematic differences due to different data processing for the eddy covariance method are negligible, and the random flux error follows a double exponential distribution even in urban areas. Notably, the relative random flux errors in the urban-influenced areas are larger than those in the forest and cropland, indicating that the direct measurement of CO_2 fluxes is more challenging in urban areas than in natural vegetation or cropland.

Our analysis demonstrates that the urban residential and suburban areas are constant CO_2 sources throughout the year, but cropland and SF areas are strong CO_2 sinks. The carbon uptake by the cropland is comparable to the SF because of the suitable climate and double-crop rotation during the study period. Our study also



demonstrates that vegetation at all the sites responds to the summer monsoon and influences seasonal changes in the strengths of carbon sources and sinks. The heavy rain spells during the summer season influence all the sites by decreasing the photosynthetic carbon uptake due to the reduction of solar radiation (i.e., mid-season depression), which has been reported in natural vegetative canopies in this region. Furthermore, the diurnal and seasonal variations of net CO₂ exchanges are also modulated in urban and suburban areas, just as they are in the cropland and forest canopy along the seasonal progression of the East Asian summer monsoon. Indeed, net CO₂ flux in the urban and suburban sites increases during the summer monsoon season with the depression of carbon uptake in the monsoon season as urban vegetation responds to the monsoon climate.

The magnitudes of net CO₂ emission and their temporal dynamics show differences between these two urban-influenced sites despite the similar climate conditions. The net CO₂ emissions per capita in the urban and suburban areas are 0.7 and 4.9 t CO₂ year⁻¹ person⁻¹, respectively. These values are smaller than those from an inventory analysis of typical Korean cities, which indicates that vegetation in the urban and suburban areas offsets the fossil fuel emissions of CO₂, indicating large uncertainties in urban scale anthropogenic CO₂ emission. The absolute magnitude of net CO₂ exchange in the high-rise residential area is smaller than those in other urban sites of similar or smaller population density (<4700 inh km⁻²) and inventory analyses based on fossil fuel emissions (e.g., [7, 48, 49, 51]). We speculate that this small value is related to the CO₂ mitigation of urban vegetation and to the district heating system. Despite the high vegetation fraction and scattered buildings, the net CO₂ emission per capita in the suburban area is considerably larger than in the high-rise high-density residential area in this study and other cities of similar vegetation fraction, possibly because of the heavy traffic volume and factories around the suburban site.

The limitations of this study notwithstanding, our findings have important policy implications for urban regeneration and energy consumption in East Asia, where rapid urbanization has been progressing for the last several decades, by indicating changes in CO₂ emission across the urbanization gradient and their controlling factors. Importantly, the urban and suburban area has a much larger relative random flux uncertainty than the other sites and previously reported vegetative canopies.

It is notable that urban vegetation mitigates anthropogenic CO₂ emissions and is influenced by the monsoon activity like natural vegetation in this region. Fossil fuel CO₂ emission data from inventory have non-negligible differences and currently several megacity carbon

projects are focusing on high-resolution mapping of CO₂ and verification of inventory data (e.g., [61, 73, 74]). Eddy covariance method has been widely used in such urban-focused projects for benchmarking and verification of fossil fuel CO₂ emissions. Our findings indicate that even in situ flux observation is challenging because of its larger random uncertainty and this larger uncertainty should be carefully considered in urban studies. Also, it is likely that a potential change in urban vegetative carbon uptake in this region might occur in response to the intensification and lengthening of the heavy rain spells in the summer growing season. Further long-term monitoring of CO₂ fluxes should be conducted with different land cover types in the East Asia region to improve our understanding of the impacts of rapid urbanization and vegetation on the carbon balance.

Abbreviations

ANN: artificial neural network; CP: double cropping cropland site; F_C: CO₂ flux; HU: high-rise residential urban site; inh: inhabitants; NEE: net ecosystem exchange of CO₂; P: population density; PAR: photosynthetically active radiation; PDF: probability density function; RH: relative humidity; SF: subtropical forest site; SU: suburban site; T_{air}: air temperature; ε: random error.

Acknowledgements

This publication was supported by the National Research Foundation of Korea grant funded by the Korean government (MSIT) (NRF-2018R1A5A1024958), and the Korea Polar Research Institute (KOPRI, PN19081). The first author was supported by the Global Ph.D. Fellowship Program (NRF-2015H1A2A1030932). Special thanks go to the editors and reviewers for their invaluable comments on this study.

Authors' contributions

J-WH and JH have made substantial contribution to the conception and design of the work, collected and analyzed the data, and drafted the manuscript. JC, YHL, L-SC, and J-BL, KY, and Y-SP, Y-HB, and SJ has made substantial contributions to collect and analyze the data from SF, HU, SU, and CP sites, respectively. All authors read and approved the final manuscript.

Funding

The fund for this publication was supported by the National Research Foundation of Korea grant funded from the Korean government (MSIT) (NRF-2018R1A5A1024958), the Korea Meteorological Administration Research and Development Program under Grant KMI2018-03512, and the Korea Polar Research Institute (KOPRI, PN19081).

Availability of data and materials

All data are available upon request to corresponding author (jhong@yonsei.ac.kr).

Ethics approval and consent to participate

Not applicable.

Consent for publication

Not applicable.

Competing interests

The authors declare that they have no competing interests.

Author details

¹ Ecosystem-Atmosphere Process Laboratory, Department of Atmospheric Sciences, Yonsei University, Yonsei-ro 50, Seodaemun-gu, Seoul 03722, South Korea. ² National Institute of Forest Science, Seoul, South Korea. ³ National Institute of Environmental Research, Incheon, South Korea. ⁴ Korea Basic

Science Institute, Cheongju, South Korea. ⁵ National Institute of Meteorological Sciences, Jeju, South Korea.

Received: 9 March 2019 Accepted: 31 August 2019

Published online: 11 September 2019

References

- Le Quéré C, Andrew RM, Friedlingstein P, Sitch S, Pongratz J, Manning AC, et al. Global carbon budget 2017. *Earth Syst Sci Data*. 2018;10:405–48.
- Andres RJ, Boden TA, Bréon FM, Ciais P, Davis S, Erickson D, et al. A synthesis of carbon dioxide emissions from fossil-fuel combustion. *Biogeosciences*. 2012;9:5.
- Martínez-Zarzoso I, Maruotti A. The impact of urbanization on CO₂ emissions: evidence from developing countries. *Ecol Econ*. 2011;70:7.
- Zhu HM, You WH, Zeng ZF. Urbanization and CO₂ emissions: a semi-parametric panel data analysis. *Econ Lett*. 2012;117:3.
- Coutts AM, Beringer J, Tapper NJ. Characteristics influencing the variability of urban CO₂ fluxes in Melbourne, Australia. *Atmos Environ*. 2007;41:1.
- Bergeron O, Strachan IB. CO₂ sources and sinks in urban and suburban areas of a northern mid-latitude city. *Atmos Environ*. 2011;45:8.
- Ward HC, Kotthaus S, Grimmond CSB, Björkegren A, Wilkinson M, Morrison WTJ, et al. Effects of urban density on carbon dioxide exchanges: observations of dense urban, suburban and woodland areas of southern England. *Environ Pollut*. 2015;198:186–200.
- Ueyama M, Ando T. Diurnal, weekly, seasonal, and spatial variabilities in carbon dioxide flux in different urban landscapes in Sakai, Japan. *Atmos Chem Phys*. 2016;16:22.
- Hong J, Kim J. Impact of the Asian monsoon climate on ecosystem carbon and water exchanges: a wavelet analysis and its ecosystem modeling implication. *Glob Change Biol*. 2011;17:1900–16.
- Hong J, Kim WS. Weather impacts on electric power load: partial phase synchronisation analysis. *Meteorol Appl*. 2015;22:811–6.
- Hong JW, Hong J, Kwon EE, Yoon DK. Temporal dynamics of urban heat island correlated with the socio-economic development over the past half-century in Seoul, Korea. *Environ Pollut*. 2019. <https://doi.org/10.1016/j.envpol.2019.07.102>.
- Hsieh CI, Katul G, Chi TW. An approximate analytical model for footprint estimation of scalar fluxes in thermally stratified atmospheric flows. *Adv Water Resour*. 2000;23:765–72.
- Trewartha GT, Horn LH. An introduction to climate. New York: McGraw-Hill; 1980.
- Hong JW, Hong J. Changes in the Seoul metropolitan area urban heat environment with residential redevelopment. *J Appl Meteorol Clim*. 2016;55:5.
- Hong JW, Lee SD, Hong J, Bong YS, Shin WJ, Yi K, Chun J. Energy, water, and carbon exchanges over the suburban area in Korea. In: Proceedings of the anniversary spring meeting of Korean meteorological society; 2016.
- Hong JW, Lee SD, Lee J, Hong J, Shin S, Park Y, Ha J, Lim E. Analysis of atmospheric phenomena in the atmospheric boundary layer using the observation at the Boseong meteorological tower. In: Proceedings of the anniversary fall meeting of Korean meteorological society; 2017.
- Papale D, Reichstein M, Aubinet M, Canfora E, Bernhofer C, Kutsch W, et al. Towards a standardized processing of Net Ecosystem Exchange measured with eddy covariance technique: algorithms and uncertainty estimation. *Biogeosciences*. 2006;3:4.
- Hollinger DY, Richardson AD. Uncertainty in eddy covariance measurements and its application to physiological models. *Tree Physiol*. 2005;25:873–85.
- Mann J, Lenschow DH. Errors in airborne flux measurements. *J Geophys Res*. 1994;99:14519–26.
- Richardson AD, Mahecha MD, Falge E, Kattge J, Moffat AM, Papale D, et al. Statistical properties of random CO₂ flux measurement uncertainty inferred from model residuals. *Agric For Meteorol*. 2008;148:1.
- Richardson AD, Hollinger DY, Burba GG, Davis KJ, Flanagan LB, Katul GG, et al. A multi-site analysis of random error in tower-based measurements of carbon and energy fluxes. *Agric For Meteorol*. 2006;136:1–8.
- Kwon H, Kim J, Hong J, Lim JH. Influence of the Asian monsoon on net ecosystem carbon exchange in two major ecosystems in Korea. *Biogeosciences*. 2010;7:1493–504.
- Hong J, Takagi K, Ohta T, Kodama Y. Wet surface resistance of forest canopy in monsoon Asia: implications for eddy covariance measurement of evapotranspiration. *Hydrol Process*. 2014;28:37–42.
- Wilczak JM, Oncley SP, Stage SA. Sonic anemometer tilt correction algorithms. *Bound Lay Meteorol*. 2001;99:1.
- van Dijk A, Moene AF, De Bruin HAR. The principles of surface flux physics: theory, practice and description of the ECPACK library. Wageningen: University of Wageningen; 2004.
- Mauder M, Cuntz M, Drüe C, Graf A, Rebmann C, Schmid HP, et al. A strategy for quality and uncertainty assessment of long-term eddy-covariance measurements. *Agric For Meteorol*. 2013;169:122–35.
- Vickers D, Mahrt L. Quality control and flux sampling problems for tower and aircraft data. *J Atmos Ocean Technol*. 1997;14:3.
- Moncrieff J, Clement R, Finnigan J, Meyers T. Averaging, detrending, and filtering of eddy covariance time series. In: Lee X, Massman W, Law B, editors. *Handbook of micrometeorology*. Dordrecht: Springer; 2004. p. 7–31.
- Moncrieff JB, Massheder JM, de Bruin H, Elbers J, Friborg T, Heusinkveld B, et al. A system to measure surface fluxes of momentum, sensible heat, water vapour and carbon dioxide. *J Hydrol*. 1997;188:589–611.
- Massman WJ. A simple method for estimating frequency response corrections for eddy covariance systems. *Agric For Meteorol*. 2000;104:3.
- Massman WJ. Reply to comment by Rannik on 'A simple method for estimating frequency response for eddy systems. *Agric For Meteorol*. 2001;107:247–51.
- Horst TW. A simple formula for attenuation of eddy fluxes measured with first-order-response scalar sensors. *Bound Lay Meteorol*. 1997;82:2.
- Ibrom A, Dellwik E, Larsen SE, Pilegaard KIM. On the use of the Webb–Pearman–Leuning theory for closed-path eddy correlation measurements. *Tellus B*. 2007;59:5.
- Horst TW, Lenschow DH. Attenuation of scalar fluxes measured with spatially-displaced sensors. *Bound Lay Meteorol*. 2009;130:2.
- Fratini G, Ibrom A, Arriga N, Burba G, Papale D. Relative humidity effects on water vapour fluxes measured with closed-path eddy-covariance systems with short sampling lines. *Agric For Meteorol*. 2012;165:53–63.
- Miyata A, Leuning R, Denmead OT, Kim J, Harazono Y. Carbon dioxide and methane fluxes from an intermittently flooded paddy field. *Agric For Meteorol*. 2000;102:4.
- Gao Z, Bian L, Zhou X. Measurements of turbulent transfer in the near-surface layer over a rice paddy in China. *J Geophys Res*. 2003. <https://doi.org/10.1029/2002JD002779>.
- Moon BK, Hong J, Lee BR, Yun JI, Park EW, Kim J. CO₂ and energy exchange in a rice paddy for the growing season of 2002 in Hari, Korea. *Korean J Agric For Meteorol*. 2003;5:2.
- Saito M, Miyata A, Nagai H, Yamada T. Seasonal variation of carbon dioxide exchange in rice paddy field in Japan. *Agric For Meteorol*. 2005;135:1.
- Muramatsu K, Ono K, Soyama N, Thanyapraneeekul J, Miyata A, Mano M. Determination of rice paddy parameters in the global gross primary production capacity estimation algorithm using 6 years of JP-MSE flux observation data. *J Agr Meteorol*. 2017;73:3.
- Schmid HP, Grimmond CSB, Cropley F, Offerle B, Su HB. Measurements of CO₂ and energy fluxes over a mixed hardwood forest in the mid-western United States. *Agric For Meteorol*. 2000;103:4.
- Turner D, Urbanski S, Bremer D, Wofsy S, Meyers T, Gower S, Gregory M. A cross-biome comparison of daily light use efficiency for gross primary production. *Glob Change Biol*. 2003;9:383–95.
- Arrhenius S. *Worlds in the making: the evolution of the universe*. Manhattan: Harper & brothers; 1908.
- Davidson EA, Janssens IA, Luo Y. On the variability of respiration in terrestrial ecosystems: moving beyond Q₁₀. *Glob Change Biol*. 2006;12:2.
- Liu HZ, Feng JW, Järvi L, Vesala T. Four-year (2006–2009) eddy covariance measurements of CO₂ flux over an urban area in Beijing. *Atmos Chem Phys*. 2012;12:17.
- Moriwaki R, Kanda M. Seasonal and diurnal fluxes of radiation, heat, water vapor, and carbon dioxide over a suburban area. *J Appl Meteorol*. 2004;43:1700–10.
- Pawlak W, Fortuniak K, Siedlecki M. Carbon dioxide flux in the centre of Łódź, Poland—analysis of a 2-year eddy covariance measurement data set. *Int J Climatol*. 2011;31:232–43.

48. Kleingeld E, van Hove B, Elbers J, Jacobs C. Carbon dioxide fluxes in the city centre of Arnhem. A middle-sized Dutch city. *Urban Clim*. 2018;24:994–1010.
49. Björkegren A, Grimmond CSB. Net carbon dioxide emission from central London. *Urban Clim*. 2018;23:131–58.
50. Fragkias M, Lobo J, Strumsky D, Seto KC. Does size matter? Scaling of CO₂ emissions and US urban areas. *PLoS ONE*. 2013;8:6.
51. Moran D, Kanemoto K, Jiborn M, Wood R, Többen J, Seto KC. Carbon footprints of 13000 cities. *Environ Res Lett*. 2018;13:064041.
52. Oda T, Maksyutov S, Andres RJ. The open-source data inventory for anthropogenic CO₂, version 2016 (ODIAC2016): a global monthly fossil fuel CO₂ gridded emissions data product for tracer transport simulations and surface flux inversions. *Earth Syst Sci Data*. 2016;2018:10.
53. Velasco E, Roth M, Tan SH, Quak M, Nabarro SDA, Norford L. The role of vegetation in the CO₂ flux from a tropical urban neighbourhood. *Atmos Chem Phys*. 2013;13:20.
54. Vesala T, Järvi L, Launiainen S, Sogachev A, Rannik Ü, Mammarella I, et al. Surface-atmosphere interactions over complex urban terrain in Helsinki, Finland. *Tellus B*. 2008;60:2.
55. Hirano T, Sugawara H, Murayama S, Kondo H. Diurnal variation of CO₂ flux in an urban area of Tokyo. *Scientific Online Lett Atmos*. 2015;11:100–3.
56. Christen A, Coops NC, Crawford BR, Kellett R, Liss KN, Olchowski I, et al. Validation of modeled carbon-dioxide emissions from an urban neighborhood with direct eddy-covariance measurements. *Atmos Environ*. 2011;45:33.
57. Raupach MR, Marland G, Cias P, Le Quéré C, Canadell JG, Klepper G, Field CB. Global and regional drivers of accelerating CO₂ emissions. *Proc Nat Acad Sci*. 2007;104:10288–93.
58. Andres RJ, Boden TA, Higdon D. A new evaluation of the uncertainty associated with CDIAC estimates of fossil fuel carbon dioxide emission. *Tellus B*. 2014;66:1.
59. Gurney KR, Liang J, O’Keeffe D, Patarasuk R, Hutchins M, Huang J, Rao P, Song Y. Comparison of global downscaled versus bottom-up fossil fuel CO₂ emissions at the urban scale in four U.S. urban areas. *J Geophys Res*. 2019;124:5.
60. Oda T, Bun R, Kinakh V, Topylko P, Halushchak M, Marland G, et al. Errors and uncertainties in a gridded carbon dioxide emissions inventory. *Mitig Adapt Strateg Glob Chang*. 2019;24:1007–50.
61. Gately CK, Hutyra LR. Large uncertainties in urban-scale carbon emissions. *J Geophys Res*. 2017;122:11–242.
62. Crawford B, Grimmond CSB, Christen A. Five years of carbon dioxide fluxes measurements in a highly vegetated suburban area. *Atmos Environ*. 2011;45:896–905.
63. Makido Y, Dhakal S, Yamagata Y. Relationship between urban form and CO₂ emissions: Evidence from fifty Japanese cities. *Urban Clim*. 2012;2:55–67.
64. Valentini R, Matteucci G, Dolman AJ, Schulze ED, Rebmann CJMEAG, Moors EJ, et al. Respiration as the main determinant of carbon balance in European forests. *Nature*. 2000;404:6780.
65. Curtis PS, Hanson PJ, Bolstad P, Barford C, Randolph JC, Schmid HP, Wilson KB. Biometric and eddy-covariance based estimates of annual carbon storage in five eastern North American deciduous forests. *Agric For Meteorol*. 2002;113:1.
66. Kato T, Tang Y. Spatial variability and major controlling factors of CO₂ sink strength in Asian terrestrial ecosystems: evidence from eddy covariance data. *Glob Change Biol*. 2008;14:10.
67. Hirata R, Saigusa N, Yamamoto S, Ohtani Y, Ide R, Asanuma J, et al. Spatial distribution of carbon balance in forest ecosystems across East Asia. *Agric For Meteorol*. 2008;148:5.
68. Takagi K, Hirata R, Ide R, Ueyama M, Ichii K, Saigusa N, et al. Spatial and seasonal variations of CO₂ flux and photosynthetic and respiratory parameters of larch forests in East Asia. *Soil Sci Plant Nutr*. 2015;61:1.
69. Lietzke B, Vogt R, Feigenwinter C, Parlow E. On the controlling factors for the variability of carbon dioxide flux in a heterogeneous urban environment. *Int J Climatol*. 2015;35:13.
70. Machimura T, Ooba M, Kikuchi Y, Oda T, Yamase K, Aoyama Y, Okada S. Annual carbon cycle of *Pinus densiflora* stand evaluated by eddy flux observation and ecological survey. *Proc AsiaFlux*; 2006.
71. Kosugi Y, Tanaka H, Takanashi S, Matsuo N, Ohte N, Shibata S, Tani M. Three years of carbon and energy fluxes from Japanese evergreen broad-leaved forest. *Agr Forest Meteorol*. 2005;132:3.
72. Matsuura S, Miyata A, Mano M, Hojito M, Mori A, Miyaji T, et al. Effects of manure application on carbon budget over managed grassland in central Japan. *Proc AsiaFlux*; 2006.
73. Newman S, Xu X, Gurney KR, Hsu YK, Li KF, Jiang X, et al. Toward consistency between trends in bottom-up CO₂ emissions and top-down atmospheric measurements in the Los Angeles megacity. *Atmos Chem Phys*. 2016;16:3843–63.
74. Turnbull JC, Karion A, Davis KJ, Lauvaux T, Miles NL, Richardson SJ, et al. Synthesis of urban CO₂ emission estimates from multiple methods from the Indianapolis Flux Project (INFLUX). *Environ Sci Technol*. 2019;53:287–95.

Publisher’s Note

Springer Nature remains neutral with regard to jurisdictional claims in published maps and institutional affiliations.

Ready to submit your research? Choose BMC and benefit from:

- fast, convenient online submission
- thorough peer review by experienced researchers in your field
- rapid publication on acceptance
- support for research data, including large and complex data types
- gold Open Access which fosters wider collaboration and increased citations
- maximum visibility for your research: over 100M website views per year

At BMC, research is always in progress.

Learn more biomedcentral.com/submissions

